12

New Multiferroic Materials: Bi_2FeMnO_6

Hongyang Zhao[1], Hideo Kimura[1], Qiwen Yao[1], Yi Du[2],
Zhenxiang Cheng[2] and Xiaolin Wang[2]
[1]*National Institute for Materials Science,*
[2]*Institute for Superconducting and Electronics Materials,*
University of Wollongong,
[1]*Japan*
[2]*Australia*

1. Introduction

The term "ferroic" was introduced by Aizu in 1970, and presented a unified treatment of certain symmetry-dictated aspects of ferroelectric, ferroelastic, and ferromagnetic materials. Ferroelectric materials possess a spontaneous polarization that is stable and can be switched hysteretically by an applied electric field; antiferroelectric materials possess ordered dipole moments that cancel each other completely within each crystallographic unit cell. Ferromagnetic materials possess a spontaneous magnetization that is stable and can be swithched hysteretically by an applied magnetic field; antiferromagnetic materials possess ordered magnetic moments that cancel each other completely within each magnetic unit cell. By the original definition, a single-phase multiferroic material is one that possesses more than one 'ferroic' properties: ferroelectricity, ferromagnetism or ferroelasticity. But the classification of multiferroics has been broadened to include antiferroic order. Multiferroic materials, in which ferroelectricity and magnetism coexist, the control of magnetic properties by an applied electric field or, in contrast, the switching of electrical polarization by a magnetic field, have attracted a great deal of interest. Now we can classify multiferroic materials into two parts: one is single-phase materials; the other is layered or composite heterostructures. The most desirable situation would be to discover an intrinsic single-phase multiferroic material at room temperature. However, $BiFeO_3$ is the only known perovskite oxides that exhibits both antiferromagnetism and ferroelectricity above room temperature. Thus, it is essential to broaden the searching field for new candidates, which resulted in considerable interest on designed novel single phase materials and layered or composite heterostructures.

2. Material designation and characterization

For ABO_3 perovskite structured ferroelectric materials, they usually show antiferromagnetic order because the same B site magnetic element. While for the $A_2BB'O_6$ double perovskite oxides, the combination between B and B′ give rise to a ferromagnetic coupling. They are also expected to be multiferroic materials. The ferroelectric polarization is induced by the distortion which usually causes a lower symmetry. For device application, a large

magnetoelectric effect is expected in the $BiFeO_3$ and bismuth-based double perovskite oxides ($BiBB'O_6$), many of which have aroused great interest like Bi_2NiMnO_6, $BiFeO_3$-$BiCrO_3$. But far as we know, few researches were focused on Bi_2FeMnO_6.

Multiferroic material is an important type of lead-free ferroelectrics. While they usually showed leaky properties and not well-shaped *P-E* loops. Dielectricity includes piezoelectricity, and piezoelectricity includes ferroelectricity. Therefore, it is essential to characterize the dielectric, piezoelectric and ferroelectric properties together. Firstly we have designed several multiferroic materials, and then we studied their properties using efficient techniques which include *P-E* loop measurement, positive-up-negative-down (PUND) test and piezoresponse force microscopy (PFM). All the fabricated materials were found to be multiferroics, so the magnetic properties were also characterized.

2.1 Material designation

Magnetism and ferroelectricity exclude each other in single phase multiferroics. It is difficult for designing multiferroics with good magnetic and ferroelectric properties. Our interest is to design new candidate multiferroics based on $BiFeO_3$. According to the Goodenough-Kanamori (GK) rules, many ferromagnets have been designed in double perovskite system ($A_2BB'O_6$) through the coupling of two B site ions with and without e_g electrons. Because the complication of the double perovskite system, there are still some questions about the violation of the GK rules in some cases and the origin of the ferromagnetism or antiferromagnetism. Nevertheless, it is believed that the B site superexchange interaction, the oxygen defects and the mixed cation valences are the important factors in determining the magnetic properties of the double perovskites. Therefore, the preparation methods and conditions will show a large influence on the magnetic properties of the fabricated double peroskites. In order to modify the antiferromagnetic properties of $BiFeO_3$, novel single-phase Bi_2FeMnO_6 series materials were designed. We have obtained very interesting results and firstly succeeded in proofing that the designed Bi_2FeMnO_6 is another promising single-phase room temperature multiferroic material. Then we designed Nd: $BiFeO_3/YMnO_3$, Nd: $BiFeO_3/Bi_2FeMnO_6$ to further study the B site superexchange interaction between Fe and Mn. Surprisingly, they also showed room temperature multiferroic properties. These exciting results provided us with more confidence in designing devices based on multiferroic materials. Different preparation methods also show large influence to their properties. The comparison between the samples of bulk, nano-powder and films is essential for the understanding of the underlying physics and the development of ferroelectric concepts.

2.1.1 Bi_2FeMnO_6 (BFM) and $(La_xBi_{1-x})_2FeMnO_6$ (LBFM)

$BiFeO_3$ is a well-known multiferroic material with antiferromagntic with a Neel temperature of 643 K, which can be synthesized in a moderate condition. In contrast, $BiMnO_3$ is ferromagnetic with T_c = 110 K and it needs high-pressure synthesis. Single phase Bi_2FeMnO_6 (BFM) ceramics could be synthesized by conventional solid state method as the target. The starting materials of Bi_2O_3, Fe_3O_4, $MnCO_3$ were weighed according to the molecular mole ratio with 10 mol% extra Bi_2O_3. They were mixed, pressed into pellets and sintered at 800 °C for 3 h. Then the ceramics were crushed, ground, pressed into pellets and sintered again at 880 °C for 1 h. BFM films were deposited on (100) $SrTiO_3$ substrate by pulsed laser deposition (PLD) method at 650°C with 500 ~ 600 mTorr dynamic oxygen.

The stabilization of the single-phase Bi-based perovskites are difficult because of their tendency of multiphase formation and the high volatility of bismuth. Stabilization can be facilitated by a partial replacement of Bi^{3+} cations by La cations. In addition, $LaMn_{1-x}Fe_xO_3$ including La_2FeMnO_6 has been also reported to be an interesting mixed-valence manganite with perovskite structure. Therefore, La was chosen to partially substitute Bi in Bi_2FeMnO_6 to stabilization the phase. Polycrystalline 20 mol% La doped Bi_2FeMnO_6 (LBFM) ceramic and film were also obtained using the similar preparation methods mentioned above.

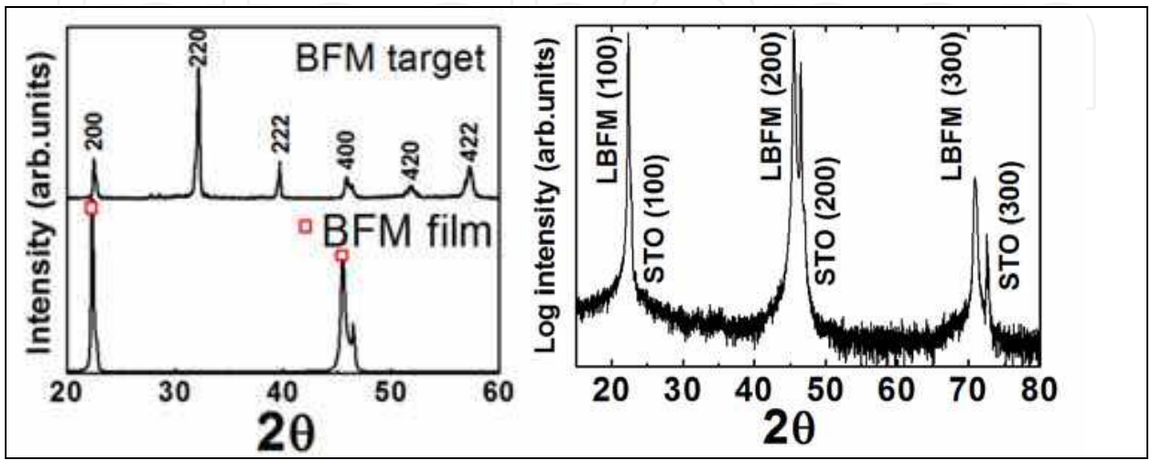

Fig. 1. XRD spectra for BFM target and film fabricated on (100) STO (left); XRD for LBFM film (right).

Figure 1 (left) shows the XRD patterns of the BFM target and the film. Because $BiFeO_3$ has a rhombohedral *R*3c structure whereas $BiMnO_3$ has a monoclinic structure, it is natural that the BFM will show a different structure due to the coexist of two transition metal octahedral with different_distortions. Bi et al has calculated three structures of BFM with the space group of $Pm3m$, *R*3 and *C*2. In this work, the bulk BFM target shows a cubic *Pm3m* structure and it was indexed using the data from Bi et al. The second phase ($Bi_2Fe_4O_9$) was observed in the BFM ceramics, which often appears in the $BiFeO_3$ ceramics. While the thin film on the (100) STO substrate fabricated in high oxygen pressure condition shows a single phase with a bulk-like structure with no traceable impurity. In this study we focused mainly on the single phase film, because the impurities will have large influences on magnetic properties and blind the observation of the intrinsic property. As shown in Figure 1 (right), the LBFM diffraction peaks of (100), (200) and (300) were observed in the XRD pattern. It indicates the epitaxial growth of LBFM film on the (100) STO substrate. There is no traceable impurity in the film which is believed to have a bulk-like cubic structure. But there are unavoidable impurities of bismuth oxides in the LBFM ceramics, which reduces further the crystalline quality of the ceramic compared with the LBFM film..

The Scanning electron microscopy (SEM) was used for the film morphology characterization. The SEM images of the BFM films were shown in Figure 2. The film on Si shows fiber shaped morphology with different orientations, as marked as parallel fibers and inclined fibers. In the contrast, the film on STO substrate shows fibers with almost the same orientation. It is essential to understand the orientation and anisotropy properties to optimize and design functional devices. In the previous work, it is proved that BFM on (100)

STO shows large magnetic anisotropy and out-of-plane is the easy magnetization direction. In this work, we focus mainly on the BFM film fabricated on STO substrates.

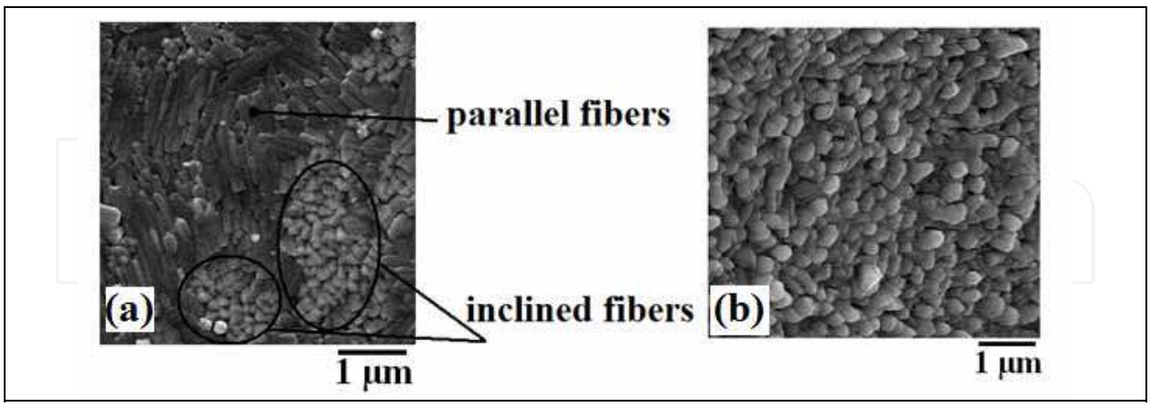

Fig. 2. SEM images of BFM film on (a) Si and (b) STO substrate.

2.1.2 Nd: $BiFeO_3$/ Bi_2FeMnO_6 (BFO/BFM)

In our former works, the doping of Nd into $BiFeO_3$ was found to further improve the ferroelectric properties. The Bilayered $Nd_{0.1}Bi_{0.9}FeO_3$ (Nd: $BiFeO_3$)/ BFM films on Pt/Ti/SiO_2/Si substrate were fabricated using a PLD system. Nd: $BiFeO_3$ films were fabricated at 550 ~ 580 °C with 200 mTorr dynamic oxygen pressure, and the BFM films were fabricated at 550 ~ 580 °C with ~10^{-5} Torr.

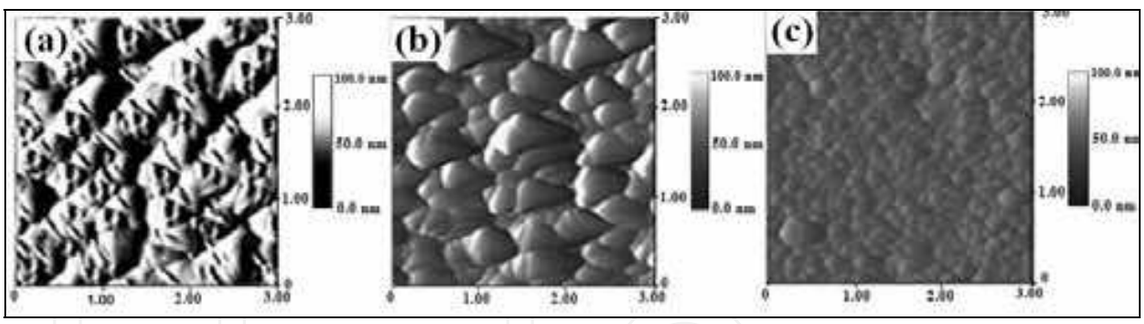

Fig. 3. Surface morphology of (a) Nd: $BiFeO_3$/Bi_2FeMnO_6, (b) Bi_2FeMnO_6 and (c) Nd: $BiFeO_3$.

The surface morphology of the Nd: $BiFeO_3$/Bi_2FeMnO_6 and Nd: $BiFeO_3$ films were studied using an atomic force microscope (AFM), as shown in Fig. 3. It can be found that the corresponding root-mean-square roughness (R_{rms}) and the grain size (S) are different: R_{rms} (Nd: $BiFeO_3$) < R_{rms} (Nd: $BiFeO_3$/Bi_2FeMnO_6) < R_{rms} (Bi_2FeMnO_6), and S (Nd: $BiFeO_3$) < S (Nd: $BiFeO_3$/Bi_2FeMnO_6) < S (Bi_2FeMnO_6). Fig. 3 (a) revealed the morphology of the Nd: $BiFeO_3$ film on the Bi_2FeMnO_6/Pt/Ti/SiO_2/Si, which indicated that Nd: $BiFeO_3$ had a larger growth rate on Bi_2FeMnO_6 than on Pt/Ti/SiO_2/Si substrate.

2.1.3 Nd: $BiFeO_3$/$YMnO_3$ (BFO/YMO)

Another well-studied muliferroic material $YMnO_3$ was chosen to from the Nd: $BiFeO_3$/$YMnO_3$ (BFO/YMO) heterostructure. The hexagonal manganite $YMnO_3$, which shows an antiferromagnetic transition at T_N=75 K and a ferroelectric transition at T_C=913

K, is one of the rare existing single phase multiferroics. The hexagonal $YMnO_3$ is ferroelectric, but the orthorhombic YMnO3 is not ferroelectric. The (111) planes are special for $BiFeO_3$, the Fe spins are coupled ferromagnetically in the pseudocubid (111) planes and antiferromagnetically between neighbouring (111) planes. In this study, the BFO/YMO film was fabricated on (111) Nb: $SrTiO_3$ (STO) substrate the Nd: $BiFeO_3$ and $YMnO_3$ ceramics were synthesized by conventional solid state method as the targets. The Nd: $BiFeO_3$/$YMnO_3$ (BFO/YMO) film were deposited on (111) STO substrate using a pulsed laser deposition (PLD) system at 530-700°C with 10^{-3} ~10^{-1} Torr dynamic oxygen. The two separate targets were alternately switched and the films were obtained through a layer-by-layer growth mode. After deposition, the film was annealed at the same condition for 15 minutes and then cooled to room temperature. In this report, the film comprised of four layers: (1) Nd: $BiFeO_3$ (2) $YMnO_3$ (3) Nd: $BiFeO_3$ and (4) $YMnO_3$. The deposition time of each layer is 10 min.

2.2 Ferroelectric characterization

The methods and special techniques for materials with weak ferroelectric properties will be explained and summarized in detail. For typical ferroelectric materials, it is easy to identify their ferroelectricity because we could obtain well-shaped ferroelectric polarization hysteresis loops (*P-E* loop). However, as the definition of ferroelectricity is strict, it is difficult to characterize weak ferroelectricity and to check whether it has ferroelectric property or not. Here we will introduce our experience for characterization and identification of such materials.

2.2.1 P-E loop measurement

For the P-E loop measurment, Pt upper electrode with an area of 0.0314 mm^2 were deposited by magnetron sputtering through a metal shadow mask. The ferroelectric properties were measured at room temperature by an aixACCT EASY CHECK 300 ferroelectric tester. Figure 4 shows the ferroelectric hysteresis loops of the Nd: $BiFeO_3$/Bi_2FeMnO_6 film, the upper inset shows the polarization fatigue as a function of switching cycles up to 10^8 and the lower inset shows frequency dependence of the real part of dielectric permittivity. The remnant polarization P_r is 54 μC/cm^2 and E_c is 237 kV/cm. Some anomalies were observed in the P-E loop: the loop is asymmetry and the polarization decreased as the increasing of the electric field. It can be caused by many effects but some of them can be neglected like the macroscopic electrode influence and nonuniform polarization on the surface of the film. We consider there are two main reasons. The film is insulating so there is no movable carriers to balance the bound charge. Therefore, the polarization gradient will be arisen in the film and induced the depolarization field. In addition, there are inhomogeneous domains with different coercivity in the film, some of which are difficult to switch with applied field. Evidence can also be seen in the fatigue results which showed that the polarization increased with the increasing of the switching cycles. The fatigue can be caused by domain nucleation, domain wall pinning due to space charges or oxygen vacancies, interface between electrode and film, thermodynamic history of the sample and so on. For the unusual profile of fatigue (polarization increased with that the increasing of switching cycles), we consider the different domain wall played important roles during the polarization reversal. The dielectric properties were measured using a HP4248 LCR meter. Frequency dependence of the real part of the permittivity was measured at room

temperature. There is a notable increase at low frequencies (as shown in the lower inset of Fig. 4). In such bilayered films, it is believed that there are space charges at the interface between the two layers of the Nd: $BiFeO_3$ and Bi_2FeMnO_6 which will affect the ferroelectric properties.

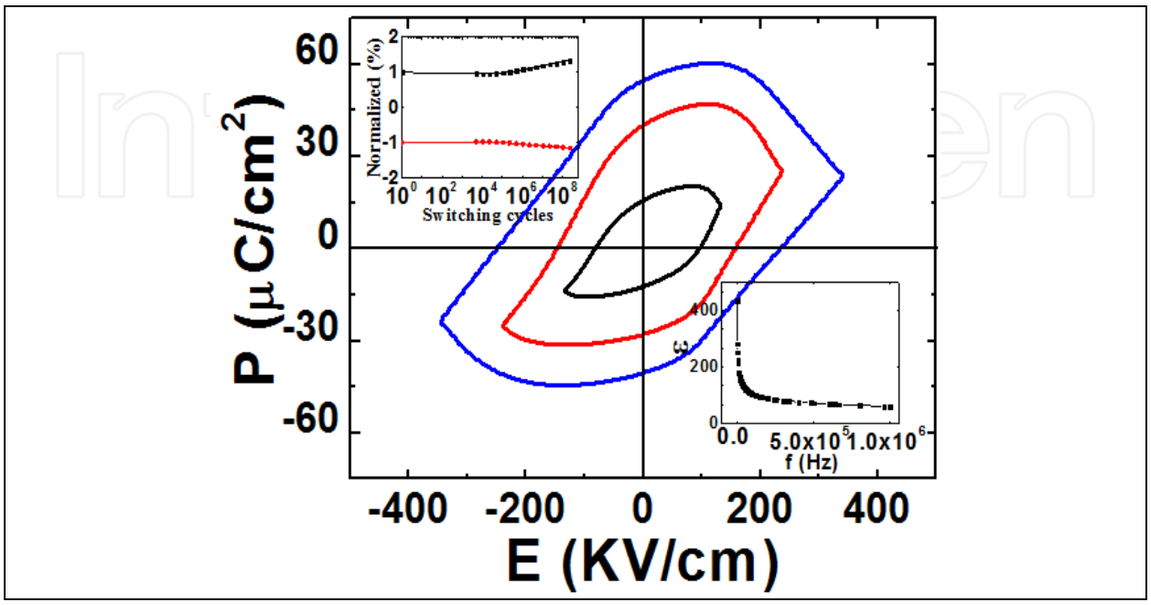

Fig. 4. Ferroelectric hysteresis loops of Nd: $BiFeO_3$/BFM film, the polarization fatigue as a function of switching cycles (upper inset) and the frequency dependence of the real part of dielectric permittivity (lower inset).

2.2.2 PUND: positive-up-negative-down test

As the definition of ferroelectricity is strict, a not-well-saturated loop might not be a proof of ferroelectricity, we have also measured the so-called positive-up-negative-down (PUND) test for Nd: $BiFeO_3$/ BFM film. The applied voltage waveform is shown in Fig. 5. The switching polarization was observed using the triangle waveform as a function of time as shown in Fig. 5.

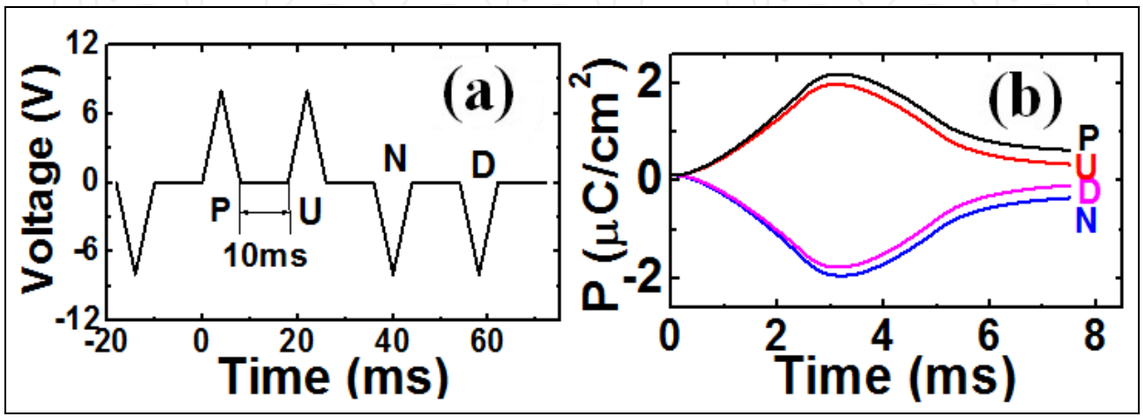

Fig. 5. (a) PUND waveform and (b) corresponding switching polarization.

2.2.3 PFM characterization for BFM and LBFM film

Until now there is no report about the ferroelectric properties of BFM because the difficulty of obtaining well-shaped polarization hysteresis loops. Thus, it is important to study and understand the ferroelectric properties and leakage mechanisms in the BFM system. The emerging technique of piezoresponse force microscopy (PFM) is proved to be a powerful tool to study piezoelectric and ferroelectric materials in such cases and extensive contributions have been published. In PFM, the tip contacts with the sample surface and the deformation (expansion or contraction of the sample) is detected as a tip deflection. The local piezoresponse hysteresis loop and information on local ferroelectric behavior can be obtained because the strong coupling between polarization and electromechanical response in ferroelectric materials. In the present study, we attempts to use PFM to study the ferroelectric/piezoelectric properties in BFM and LBFM thin films. PFM response was measured with a conducting tip (Rh-coated Si cantilever, k~1.6 N m^{-1}) by an SII Nanotechnology E-sweep AFM. PFM responses were measured as a function of applied DC bias (V_{dc}) with a small ac voltage applied to the bottom electrode (substrate) in the contact mode, and the resulting piezoelectric deformations transmitted to the cantilever were detected from the global deflection signal using a lock-in amplifier.

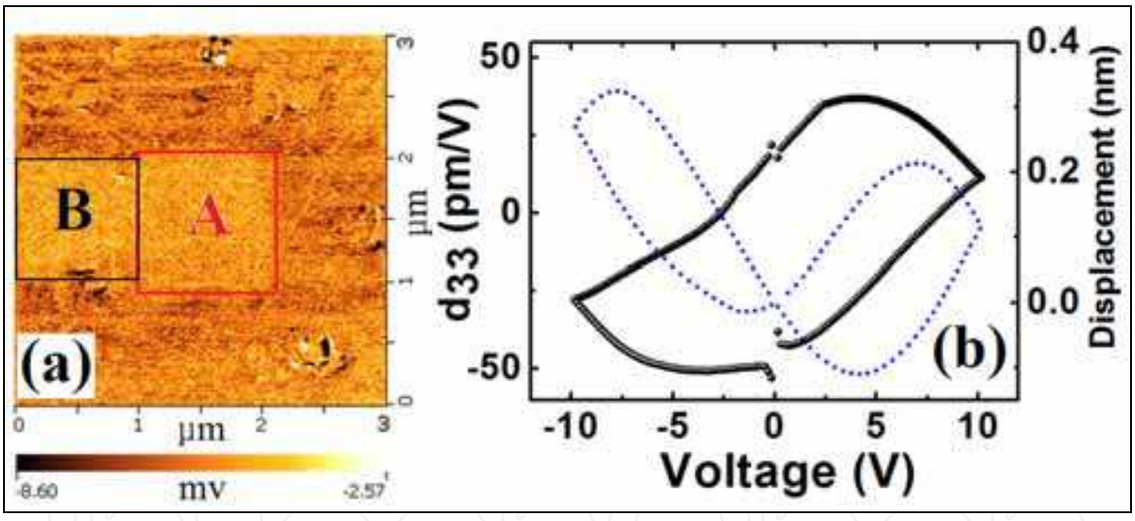

Fig. 6. (a) OP PFM image polarized by ±10 V and (b) which curve is associated with the left y-axis and which one is with the right y-axis as well as Fig.7 (c)local piezoresponse hysteresis loop of BFM film.

In Figure 6 (a), the smaller part A marked in red square was firstly poled with -10 V DC bias, and the total area of 3×3 μm² was subsequently poled with +10 V DC bias. The domain switching in red square area was observed, while another similar area beside 'A' was also observed and marked as B in black square. It may be because the expansion of ferroelectric domain under the DC bias. To further understand its ferroelectric nature, the local piezoelectric response was measured with a DC voltage from -10 V to 10 V applied to the sample. The typical "butterfly" loop was observed but it is not symmetrical, and it is not well-shaped due to the asymmetry of the upper and bottom electrodes. According to the equation $d_{33}=\Delta l/V$, where Δl is the displacement, the effective d_{33} could be calculated. At the voltage of -10 V, the sample has the maximum effective d_{33} of about -28 pm/V.

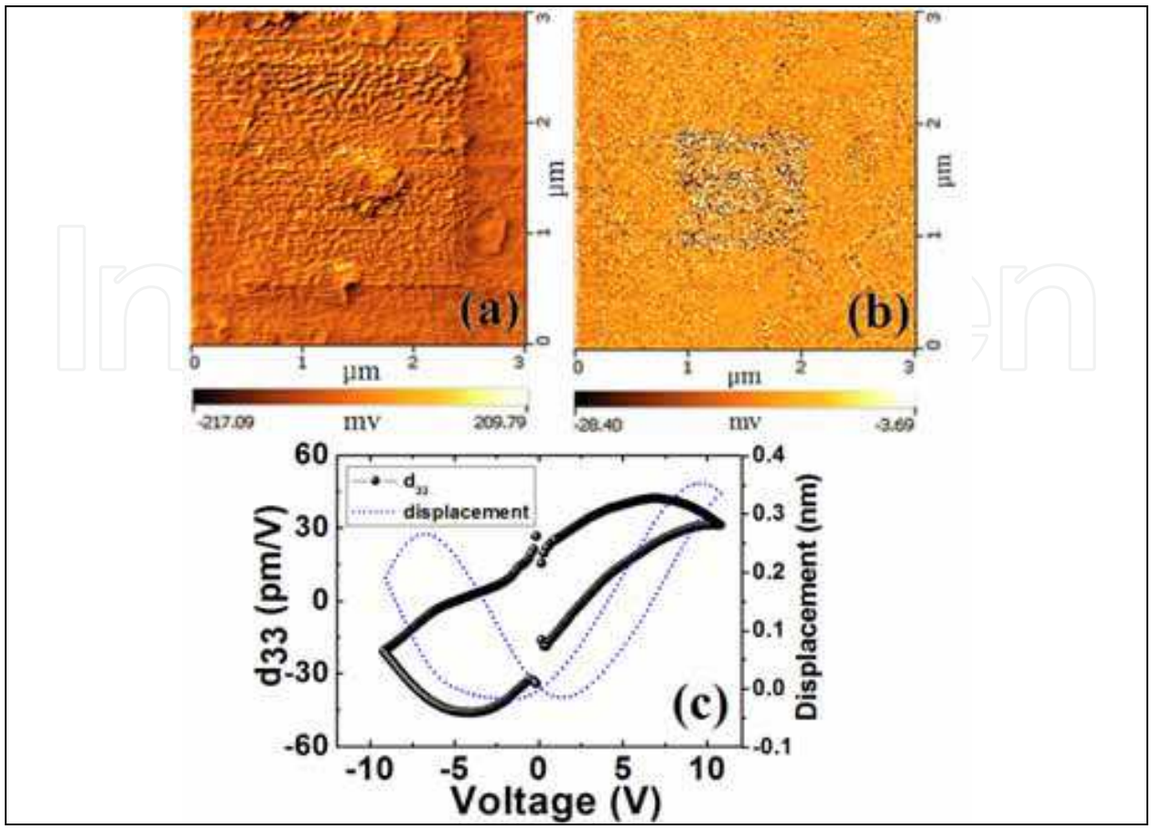

Fig. 7. (a) OP PFM image, (b) IP PFM image polarized by ±10 V and (c) local piezoresponse hysteresis loop of LBFM film.

Figure 7 shows the OP (a) and IP (b) PFM images of the LBFM film which was also fabricated on (100) STO substrate. Under ±10 V DC bias, PFM images were observed in the scans of the LBFM film, demonstrating that polarization reversal is indeed possible and proving that the LBFM film is ferroelectric at room temperature. At the voltage of 10 V, the sample has a maximum effective d_{33} of about 32 pm/V. The LBFM film shows improved piezoelectric and ferroelectric properties compared to the BFM film, indicating that through the doping or changing of other conditions, the ferroelectric property of BFM system could be improved as in the $BiFeO_3$. The domain boundary is very clear and regular in LBFM, while in BFM it is obscure and expanded over the poled area. The propagation of domain wall is strongly influenced by local inhomogeneities (e.g. grain boundaries) and stress in polycrystalline ferroelectrics, which results in strong irregularity of the domain boundary. After the La substitution, it is assumed that the crystallization is better both in ceramics and films.

2.3 Magnetic characterization for BFM film

BFM is considered to be a new multiferroic material, it is important to study their magnetic properties. Magnetic properties were measured using the commercial Quantum Design SQUID magnetometer (MPMS). In the following, we will discuss the XPS measurements, the magnetization hysteresis loops, and the ZFC and FC courves for the BFM film fabricated on the (100) STO susbtrate.

2.3.1 XPS measurements

The valance states of Fe and Mn in the BFM film were carried out using PHI Quantera SXM x-ray photoelectron spectrometer (XPS). Figure 8 shows the Fe 2p and Mn 2p photoelectron spectra of BFM film. It was reported that Fe 2p photoelectron peaks from oxidized iron are associated with satellite peaks, which is important for identifying the chemical states. The Fe^{2+} and Fe^{3+} $2p_{3/2}$ peaks always show the satellite peaks at 6 eV and 8 eV above the principal peaks at 709.5 eV and 711.2 eV, respectively. In Figure 8 (a), the satellite peaks were found just 8 eV above the $2p_{3/2}$ principal peak. It indicates that in this system Fe is mainly in the Fe^{3+} state. Figure 8 (b) shows typical XP spectra of Mn 2p. There are two main peaks corresponding to the $2p_{1/2}$ and $2p_{3/2}$ peaks, respectively. The peaks with higher binding energy above the main peaks as well as the splitting of the main peaks were observed in the film. It indicates the existence of Mn^{2+}. Such shake-up satellite peaks were considered to be a typical behavior in Mn^{2+} systems.

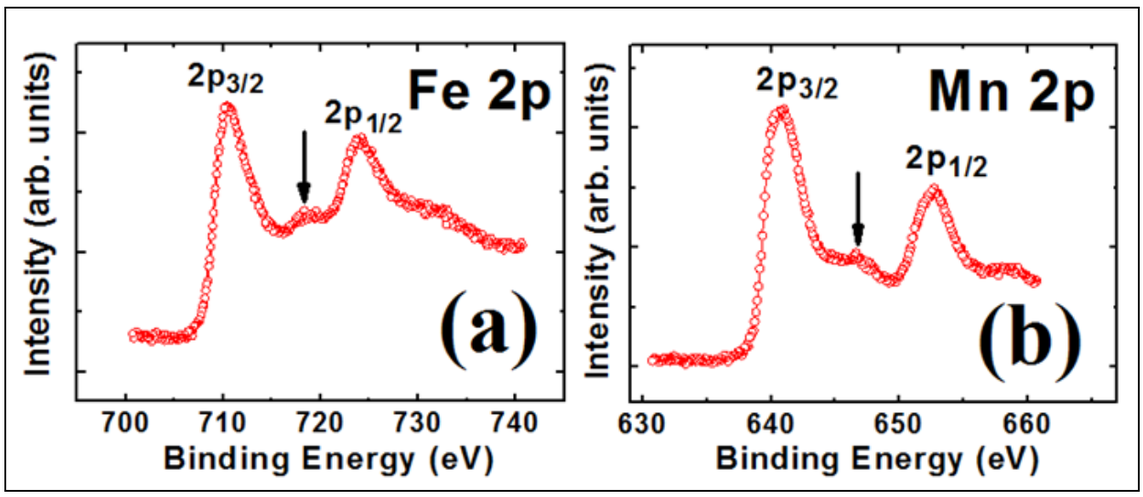

Fig. 8. (a) Fe 2p and (b) Mn 2p XP spectra for BFM film on (100) STO

2.3.2 Magnetic hysteresis loops

For the BFM thin films, different substrates of $Pt/Ti/SiO_2/Si$ and STO were used and different fabrication conditions were attempted. Some unavoidable impurities and different structures were observed for the films on $Pt/Ti/SiO_2/Si$ substrates. In order to discuss the origin of the ferromagnetic properties in BFM film, films on (100) STO were used for the study of magnetic properties. Figure 9 (a) shows the hysteresis loops measured at different temperatures. There is no significant change in the loop width from 5 K to 300 K. Figure 9 (b) shows the in-plane and out-of-plane magnetic field dependence of magnetization measured at 5 K. The film shows stress induced anisotropy from film/substrate mismatch which is an evidence of a Jahn-Teller effect and the out-of-plane is the easy magnetization direction. However, we observed experimentally that Mn shows multiple valence states despite the higher stability of the compound only containing Mn^{3+} ions in the film. It is possibly because the Mn^{2+} and Mn^{4+} cations could decrease the Jahn-Teller effect from Mn^{3+} in the film, which may result in less lattice distortion caused by Mn^{3+}.

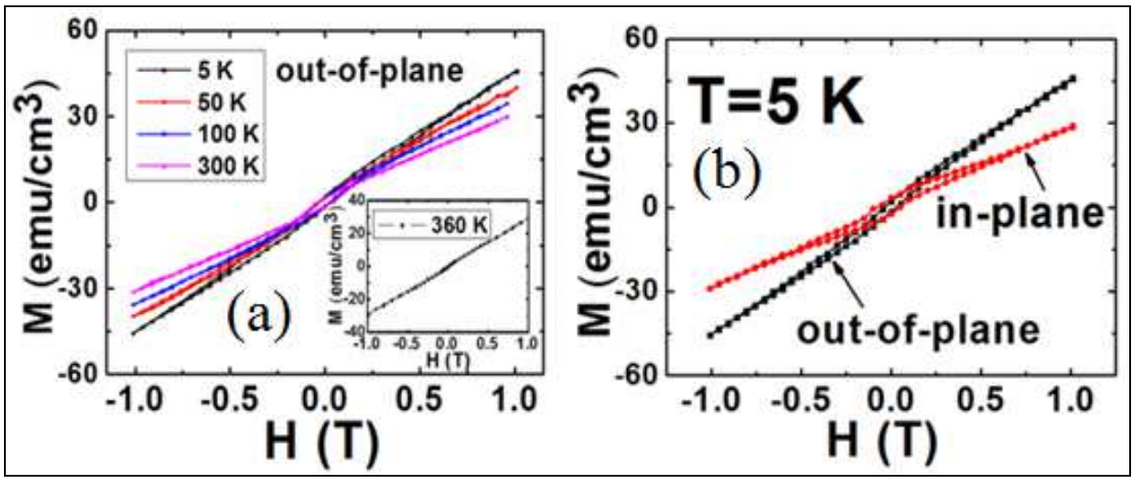

Fig. 9. Magnetic hysteresis loops of BFM film. (a) at different temperatures and (b) with magnetic field applied parallel and perpendicular to the sample plane

2.3.3 ZFC and FC measurements

Figure 10 shows temperature dependence of out-of-plane magnetization measured under zero-field-cooling (ZFC) and field-cooling (FC) conditions and in different magnetic fields. Similar to $BiFeO_3$ (with a cusp at around 50 K) a spin-glass-like behavior below 100 K was observed with the cusp at about 25 K. As shown in Figure 10 (a), the irreversibility below 100 K between FC curve and ZFC curve is clear with applied field of 500 Oe and 1000 Oe, but it was suppressed in higher field above 5 kOe and shift to much lower temperature, which is a typical behavior of spin glass ordering. Above the temperature of 100 K for spin-glass-like behavior appearing, another magnetic transition at about 360 K was observed in Figure 10 (b). Hysteresis behavior disappears above this temperature as shown in Figure 9 (a), which indicated an antiferromagnetic transition happens at this temperature.

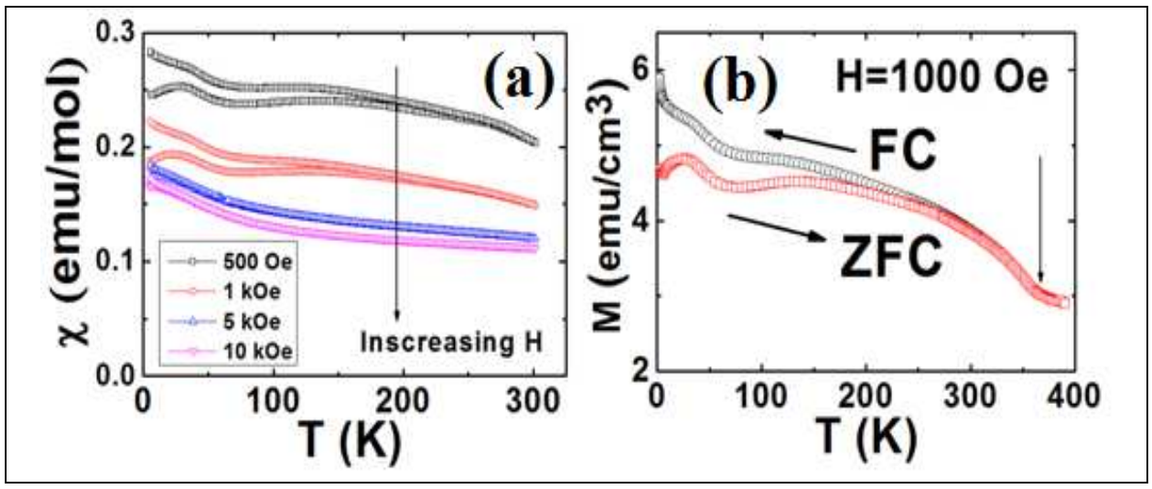

Fig. 10. ZFC and FC results of BFM film.

The film on STO was fabricated at higher temperature and higher oxygen pressure resulted in a good crystalline quality, less oxygen vacancies and no traceable impurity. BFM film on

(100) STO made under these improved fabrication conditions will display enhanced magnetic properties. The magnetizations of BFM film at 1 T are estimated from *M-H* loops as 0.30 μ_B, 0.26 μ_B, 0.23 μ_B, 0.21 μ_B and 0.19 μ_B per B site ion at temperatures of 5 K, 50 K, 100 K, 300 K and 360 K, respectively. These values are smaller than 0.5 μ_B for antiferromagnetic ordering of Fe^{3+} and Mn^{3+}, which is probably due to the local inhomogeneities in the film and some antisite disorders in the B-site. Actually the magnetic moment should be much larger than 0.5 μ_B at per B site if Mn and Fe are homogenously distributed, because both Fe^{3+}-O^{2-}-Mn^{2+} and Fe^{3+}-O^{2-}-Mn^{3+} in 180-degree bonds will produce orthoferrite, i.e. canted antiferromagnet and result in a larger moment based on the Goodenough-Kanamori rules. Therefore, in our films the arrangements of Mn^{3+}-O-Mn^{3+} and Fe^{3+}-O-Fe^{3+} with both resulting strong antiferromagnetism will have significant contribution to the observed magnetic properties. Due to Mn^{3+} ($3d^4$) is a Jahn-Teller ion, a strong Jahn-Teller effect will cause significant structure distortion in BFM film and produce the anisotropy effects. An external stress originating from BFM/STO lattice mismatches can greatly enhance the resulting cooperative strain and enhance the magnetic anisotropy. However, the multiple valence states of Mn ions in the film, the Mn^{2+} and Mn^{4+} can decrease the lattice distortion caused by Mn^{3+} and result in better lattice matching between film/substrate and decrease the anisotropic property. All of the curves shown here are corrected from the diamagnetic background of the STO substrate. The *M-H* and *M-T* data of the (100) STO substrate were obtained using the same system.

3. Conclusion

The piezoelectric/ferroelectric and magnetic properties of BFM series materials, which include BFM film and ceramic, LBFM film and ceramic, Nd: $BiFeO_3$/ BFM film and Nd: $BiFeO_3$/$YMnO_3$ film, were studied in detail. In this chapter, we mainly focus on the BFM film. It was proved that stabilization can be facilitated by a partial replacement of Bi^{3+} cations by La cations. The film and ceramic showed different properties and after La doping, both ferroelectric and magnetic properties were improved.

The piezoelectric/ferroelectric properties of BFM series materials have been studied using different methods, including *P-E* loop measurement, positive-up-negative-down (PUND) test and piezoresponse force microscopy (PFM). PFM was used to investigate the domain configurations and local piezoresponse hysteresis loops for BFM and LBFM films. The PFM images confirmed that the domain could be poled and switched in both films. The clearer domain boundary in the LBFM film indicated better crystallization and ferroelectric properties compared to the BFM film. The local butterfly-type piezoresponse hysteresis loops were obtained. All the observations suggest that BFM and LBFM films are room temperature ferroelectric materials. Improved ferroelectric properties are expected in the BFM system through the adjustment of doping ions and fabrication conditions to obtain promising multiferroic candidates.

The magnetic hysteresis loops and temperature dependent magnetization were also studied. BFM film with good crystalline quality and with enhanced magnetic properties was obtained on (100) $SrTiO_3$ substrate through the optimization of the fabrication conditions. Similar to $BiFeO_3$, the spin-glass-like behavior is observed below 100 K with the cusp at 25 K. The ZFC and FC curves measured from 2 K to 400 K show a kink at around 360 K and hysteresis disappears at 360 K, revealing a antiferromagnetic transition at this temperature. The observed anisotropy effects were caused by Jahn-Teller ions of Mn^{3+}. Mn tends to form

multiple valence states as in the film it is possibly because the Mn^{2+} and Mn^{4+} cations decrease the Jahn-Teller effect caused by Mn^{3+}.
Several questions in weak ferroelectric materials still remained to be anwsered. We wish to share these questions and have more discussion based on the as-designed materials for further development of such ferroelectrics.

4. Acknowledgment

The authors gratefully acknowledge Dr. Shigeki Nimori, Dr. Hideaki Kitazawa, Dr. Minora Osada, Dr. Baowen Li of NIMS, Prof. Huarong Zeng of Shanghai Institute of Ceramics for the valuable discussions and Dr. Hideo Iwai of NIMS for the XPS measurement. This work was supported in part by grants from JSPS and ARC under the Japan-Australia Research Cooperative Program, and Grant-in-Aid for JSPS Fellows (21-09608).

5. References

Lines, M.E. & A.M. Glass, (1977), *Principles and applications of ferroelectrics and related materials,* Oxford University press, ISBN 0198512864

Eerenstein,W.; Mathur, N.D. & Scott, J.F. (2006). Multiferroic and magnetoelectric materials. *Nature,*Vol. 442, No. 17, (August 2006), pp. 759-765, ISSN 0028-0836

Dass, R. I.; Yan, J. Q. & Goodenough, J. B. (2003). Oxygen stoichiometry, ferromagnetism and transport properties of $La_{2-x}NiMnO_{6+\delta}$, *Phys. Rev. B* Vol. 68, pp. 064415-064427, ISSN 1098-0121

Dass, R.I. & Goodenough, J.B. (2003). Multiple magnetic phases of $La_2CoMnO_{6-\delta}$ ($0<\sim\delta<\sim0.05$), *Phys. Rev. B* Vol.67, pp. 014401.1-014401.9, ISSN 1098-0121

Blasse, G. (1965). Ferromagnetic interactions in non-metallic perovskites, *J. Phys. Chem. Solids,* Vol. 26, No. 12, pp. 1969-1971, ISSN 0022-3697

Azuma, M.; Takata, K.; Saito, T.; Ishiwata, S.; Shimakawa, Y. & Takano, M. (2005). A Designed New Ferromagnetic Ferroelectric Bi_2NiMnO_6, *J. Am. Chem. Soc.* Vol. 1, pp. 8889-8892, ISSN 0002-7863

Rogado, N.S.; Li, J.; Sleight, A.W. & Subramanian, M.A. (2005). Magnetocapacitance and Magnetoresistance Near Room Temperature in a Ferromagnetic Semiconductor: La_2NiMnO_6, *Adv. Mater.* Vol. 17, pp. 2225-2227, ISSN 1501-4095

Wang, J.; Neaton, J. B.; Zheng, H.; Nagarajan, V.; Ogale, S. B.; Liu, B.; Viehland, D.; Vaithyanathan, V.; Schlom, D. G.; Wuttig, M. & Ramesh, R. (2003). Epitaxial BiFeO3 Multiferroic Thin Film Heterostructures, *Science* Vol. 299, (March 2003), pp. 1719-1722, ISSN 0036-8075

Atou, T.; Chiba, H.; Ohoyama, K.; Yamaguchi, Y. & Syono, Y. (1999). Structure Determination of Ferromagnetic Perovskite $BiMnO_3$, *J. Solid State Chem.* Vol. 145, No. 2, pp. 639-642, ISSN 0022-4596

Kimura, T.; Kawamoto, S.; Yamada, I.; Azuma, M.; Takano, M. & Tokura, Y. (2003). Magnetocapacitance effect in multiferroic $BiMnO_3$, *Phys. Rev. B* Vol. 67 (R), (May 2003), pp. 180401-180404, ISSN 1098-0121

Fujino, S.; Murakami, M.; Lim, S. H.; Salamanca-Riba, L.G.; Wuttig, M. & Takeuchi, I. (2007). Multiphase growth in Bi-Mn-O thin films, *J. Appl. Phys.* Vol. 101, No. 1, pp. 013903, ISSN 0021-8979

De, K.; Ray, R.; Panda, R.N.; Giri. S.; Nakamura, H. & Kohara, T. (2005). The effect of Fe substitution on magnetic and transport properties of $LaMnO_3$, *J. Magn. Magn. Mater.* Vol. 288, pp. 339-346, ISSN 0304-8853

De, K.; Thakur, M.; Manna, A. & Giri, S. (2006). Unusual glassy states in $LaMn_{0.5}Fe_{0.5}O_3$: Evidence of two distinct dynamical freezing processes, *J. Appl. Phys.* Vol. 99, No. 1, pp. 013908, ISSN 0021-8979

Tong, W.; Zhang, B.; Tan, S. & Zhang, Y. (2004). Probability of double exchange between Mn and Fe in $LaMn_{1-x}Fe_xO_3$, *Phys. Rev. B* Vol. 70, (July 2004), pp. 014422, ISSN 1098-0121

Gajek, M.; Bibes, M.; Fusil, S.; Bouzehouane, K.; Fontcuberta, J.; Barthelemy, A. & Fert, A. (2007). Tunnel junctions with multiferroic barriers, *Nat. Mater.* Vol. 6, pp. 296-302, ISSN 1476-1122

Gajek, M.; Bibes, M.; Wyczisk, F.; Varela, M.; Fontcuberta, J. & Barthelemy, A. (2007). Growth and magnetic properties of multiferroic $La_xBi_{1-x}MnO_3$ thin films, *Phys. Rev. B* Vol. 75, (May 2007), pp. 174417, ISSN 1098-0121

Langenberg, E.; Varela, M.; Garcia-Cuenca, M.V.; Ferrater, C.; Polo, M.C.; Fina, I.; Fabrega, L.; Sanchez, F. & Fontcuberta, J. (2009). Epitaxial thin films of $(Bi_{0.9}La_{0.1})_2NiMnO_6$ obtained by pulsed laser deposition, *J. Mag. Mag. Mat.* Vol. 321, No. 11, pp. 1748-1753, ISSN 0304-8853

Marin, L.W.; Crane, S.P.; Chu, Y-H.; Holcomb, M.B.; Gajek, M.; Huijben, M.; Yang, C-H.; Balke, N. & Ramesh, R. (2008). Multiferroics and magnetoelectrics: thin films and nanostructures, *J. Phys.: Condens. Matter* Vol. 20, No. 43, pp. 434220, ISSN 1742-6588

Yakel, H.L.; Koehler, W.C.; Bertaut, E.F.& Forrat, E.F. (1963). On the crystal structure of the manganese(III) trioxides of the heavy lanthanides and yttrium, *Acta Crystallogr.* Vol. 16 pp. 957-962, ISSN 0365-110X

Dho, J.; Leung, C.W.; MacManus-Driscoll, J.L. & Blamire, M.G. (2004). Epitaxial and oriented $YMnO_3$ film growth by pulsed laser deposition, *J. Crystal Growth* Vol. 267, No. 3-4, pp. 548-553, ISSN 0022-0248

Ruette, B.; Zvyagin, S.; Pyatakov, A.P.; Bush, A.; Li, J.F.; Belotelov, V.I.; Zvezdin, A.K. & Viehland, D. (2004). Magnetic-field-induced phase transition in $BiFeO_3$ Cycloidal to homogeneous spin observed by high-field electron spin resonance: order, *Phys. Rev. B* Vol. 69, (February 2004), pp. 064114, ISSN 1098-0121

Jang, H.W.; Ortiz, D.; Baek, S.; Foliman, C.M.; Das, R.R.; Shafer, P.; Chen, Y.B.; Nelson, C.T.; Pan, X.Q.; Ramesh, R. & Eom, C. (2009). Domain Engineering for Enhanced Ferroelectric Properties of Epitaxial (001) BiFeO Thin Films, *Adv. Mater.* Vol. 21, No. 7, pp. 817-823, ISSN 1501-4095

Wu, J.G.; Kang, G.Q.; Liu H. J. &Wang, J. (2009). Ferromagnetic, ferroelectric, and fatigue behavior of (111)-oriented $BiFeO_3/(Bi_{1/2}Na_{1/2})TiO_3$ lead-free bilayered thin films, *Appl. Phys. Lett.* Vol. 94, No. 17, pp. 172906, ISSN 0003-6951

Scott, J.F. (2008). Ferroelectrics go bananas, *J. Phys: Condens. Matter,* Vol. 20, No. 2, pp. 021001, ISSN 1742-6588

Scott, J. F. (2000). *Ferroelectric memories,* Springer, ISBN 978-3-540-66387-4, Berlin

Balke, N.; Bdikin, I.; Kalinin, S.V. & Kholkin, A.L. (2009). Electromechanical Imaging and Spectroscopy of Ferroelectric and Piezoelectric Materials: State of the Art and Prospects for the Future, *J. Am. Ceram. Soc.,* Vol. 92, No. 8, pp. 1629-1647, ISSN 1551-2916

Kalinin, S.V. & Bonnell, D.A. (2001). Local potential and polarization screening on ferroelectric surfaces, *Phys. Rev. B* Vol. 63, (March 2001), pp. 125411, ISSN 1098-0121

Kalinin, S.V.; Rodriguez, B.J.; Borisevich, A.Y.; Baddorf, A.P.; Balke, N.; Chang, H.J.; Chen, L.Q.; Choudhury, S.; Jesse, S.; Maksymovych, P.;. Nikiforov, M.P & Pennycook, S.J.

(2010). Defect-Mediated Polarization Switching in Ferroelectrics and Related Materials: From Mesoscopic Mechanisms to Atomistic Control *Adv. Mater.* Vol. 22, No. 3, pp. 314-322, ISSN 1501-4095

Shafer, P.; Zavaliche, F.; Chu, Y.H.; Yang, P.L.; Cruz, M.P. & Ramesh, R. (2007). Planar electrode piezoelectric force microscopy to study electric polarization switching in $BiFeO_3$, *Appl. Phys. Lett.* Vol. 90, pp. 202909, ISSN 0003-6951

Catalan, G.; Bea, H.; Fusil, S.; Bibes, M.; Paruch, P.; Barthélémy, A. & Scott, J.F. (2008). Fractal Dimension and Size Scaling of Domains in Thin Films of Multiferroic $BiFeO_3$, *Phy. Rev. Lett.* Vol. 100, No. 2, pp. 027602, ISSN 0031-9007

Keeney, L.; Zhang, P.F.; Groth, C.; Pemble, M.E. & Whatmore, R.W. (2010). Piezoresponse force microscopy investigations of Aurivillius phase thin films, *J. Appl. Phys.* Vol. 108, pp. 042004, ISSN 0021-8979

Cheng, Z.X.; Wang, X.L.; Dou, S. X.; Kimura, H. & Ozawa, K. (2008). Improved ferroelectric properties in multiferroic $BiFeO_3$ thin films through La and Nb codoping, *Phys. Rev. B* Vol. 77, pp. 092101, ISSN 1098-0121

Cheng, Z.X.; Li, A.H.; Wang, X.L.; Dou, S.X.; Ozawa, K.; Kimura, H.; Zhang, S.J. & Shrout, T.R. (2008). Structure, ferroelectric properties, and magnetic properties of the La-doped bismuth ferrite, *J. Appl. Phys.* Vol. 103, pp. 07E507, ISSN 0021-8979

Zhao, H.Y.; Kimura, H.; Cheng, Z.X.; Wang, X.L. &Nishida, T. (2009). Room temperature multiferroic properties of Nd:$BiFeO_3$/Bi_2FeMnO_6 bilayered films, *Appl. Phys. Lett.* Vol. 95, No. 23, pp. 232904, ISSN 0003-6951

Zhao, H.Y.; Kimura, H.; Cheng, Z.X.; Wang, X.L.; Ozawa, K. & Nishida, T. (2010). Magnetic characterization of Bi_2FeMnO_6 film grown on (100) $SrTiO_3$ substrate *Phys. Status Solidi RRL* Vol. 4, No. 11, pp. 314, ISSN 1862-6270

Zhao, H.Y.; Kimura, H.; Cheng, Z.X.; Wang, X.L.; Ozawa, K. & Nishida, T. (2010). Magnetic properties of La doped Bi_2FeMnO_6 ceramic and film, *J. App. Phys.* Vol. 108, pp. 093903, ISSN 0021-8979

Du, Y.; Cheng, Z.X.; Dou, S.X.; Wang, X.L.; Zhao, H.Y. & Kimura, H. (2010). Magnetic properties of Bi_2FeMnO_6: A multiferroic material with double-perovskite structure, *Appl. Phys. Lett.* Vol. 97, pp. 122502, ISSN 0003-6951

Wandelt, C. (1982). Photoemission studies of adsorbed oxygen and oxide layers, *Surf. Sci. Pep.* Vol. 2, No. 1, pp. 1-121, ISSN 0127-5729

Beyreuther, E.; Grafstrom, S.; Thiele, L.M. & Dorr, K. (2006). XPS investigation of Mn valence in lanthanum manganite thin films under variation of oxygen content, *Phys. Rev. B* Vol. 73, No. 15, pp. 155425, ISSN 1098-0121

Wang L. & Gao, J. (2009). Electronic structures and Hall effect in low-doped $La_{0.9}Hf_{0.1}MnO_3$ epitaxial films, *J. Appl. Phys.* Vol. 105, pp. 07E514, ISSN 0021-8979

Dionne, G.F. (1979). Origin of the magnetostriction effects from Mn_{3+}, Co_{2+}, and Fe_{2+} ions in ferrimagnetic spinels and garnets, *J. Appl. Phys.* Vol. 50, pp. 4263, ISSN 0021-8979

Dionne, G.F. (2007). Evidence of magnetoelastic spin ordering in dilute magnetic oxides, *J. Appl. Phys.* Vol. 101, pp. 09C509, ISSN 0021-8979

Dionne G.F. & Kim, H-S. (2008). *J. Appl. Phys.* Vol. 103, pp. 07B333, ISSN 0021-8979

Bi, L.; Taussig, A.R.; Kim, H-S.; Wang, L.; Dionne, G.F.; Bono, D.; Persson, K.; Ceder, G.& Ross, C.A. (2008). Structural, magnetic, and optical properties of $BiFeO_3$ and Bi_2FeMnO_6 epitaxial thin films: An experimental and first-principles study, *Phys. Rev. B* Vol. 78, No. 10, pp. 104106, ISSN 1098-0121

Singh, M.K.; Prelier, W.; Singh, M.P.; Katiyar, R. S. &. Scott, J. F (2008). Spin-glass transition in single-crystal $BiFeO_3$,*Phys. Rev. B* Vol. 77, No. 14, pp. 144403, ISSN 1098-0121

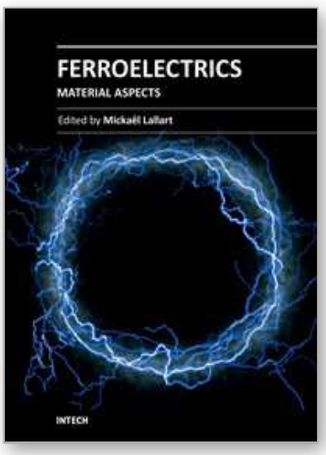

Ferroelectrics - Material Aspects

Edited by Dr. MickaÃ«l Lallart

ISBN 978-953-307-332-3
Hard cover, 518 pages
Publisher InTech
Published online 24, August, 2011
Published in print edition August, 2011

Ferroelectric materials have been and still are widely used in many applications, that have moved from sonar towards breakthrough technologies such as memories or optical devices. This book is a part of a four volume collection (covering material aspects, physical effects, characterization and modeling, and applications) and focuses on ways to obtain high-quality materials exhibiting large ferroelectric activity. The book covers the aspect of material synthesis and growth, doping and composites, lead-free devices, and thin film synthesis. The aim of this book is to provide an up-to-date review of recent scientific findings and recent advances in the field of ferroelectric materials, allowing a deep understanding of the material aspects of ferroelectricity.

INTECH
open science | open minds

InTech Europe
University Campus STeP Ri
Slavka Krautzeka 83/A
51000 Rijeka, Croatia
Phone: +385 (51) 770 447
Fax: +385 (51) 686 166
www.intechopen.com

InTech China
Unit 405, Office Block, Hotel Equatorial Shanghai
No.65, Yan An Road (West), Shanghai, 200040, China
中国上海市延安西路65号上海国际贵都大饭店办公楼405单元
Phone: +86-21-62489820
Fax: +86-21-62489821

IntechOpen